Cell PRESS
Open ACCESS

Cell Reports
Report

Dependence of Immunoglobulin Class Switch Recombination in B Cells on Vesicular Release of ATP and CD73 Ectonucleotidase Activity

Francesca Schena,[1,13] Stefano Volpi,[1,13] Caterina Elisa Faliti,[2,13] Federica Penco,[1] Spartaco Santi,[4] Michele Proietti,[2,3] Ursula Schenk,[2] Gianluca Damonte,[5] Annalisa Salis,[5,7] Marta Bellotti,[5] Franco Fais,[6] Claudya Tenca,[6] Marco Gattorno,[1] Hermann Eibel,[8] Marta Rizzi,[8] Klaus Warnatz,[8] Marco Idzko,[11] Cemil Korcan Ayata,[11] Mirzokhid Rakhmanov,[8] Thierry Galli,[9,10] Alberto Martini,[1] Marco Canossa,[4,12] Fabio Grassi,[2,3] and Elisabetta Traggiai[1,14,*]
[1]Department of Pediatrics, University of Genova and Pediatria II, Institute G Gaslini, 16148 Genova, Italy
[2]Institute for Research in Biomedicine, 6500 Bellinzona, Switzerland
[3]Dipartimento di Biologia e Genetica per le Scienze Mediche, Università di Milano, 20129 Milan, Italy
[4]Department of Neuroscience and Brain Technologies, Fondazione Istituto Italiano di Tecnologia, via Morego 30, 16163 Genova, Italy
[5]Center of Excellence for Biomedical Research (CEBR)
[6]Human Anatomy Section, Department of Experimental Medicine
[7]Department of Hearth Environmental and Life Science (DISTAV)
University of Genova, 16132 Genova, Italy
[8]Centre for Chronic Immunodeficiency, University Medical Centre Freiburg, 79106 Freiburg, Germany
[9]Institut Jacques Monod, CNRS, UMR 7592, Université Paris Diderot, Sorbonne Paris Cité, F-75205 Paris, France
[10]Membrane Traffic in Neuronal and Epithelial Morphogenesis, INSERM ERL U950, F-75013 Paris, France
[11]Department of Pneumology, University Medical Centre Freiburg, 79106 Freiburg, Germany
[12]European Brain Research Institute (EBRI), via del Fosso di Fiorano 64, 00143 Rome, Italy
[13]These authors contributed equally to this work
[14]Present address: Novartis Institute for Research in Biomedicine, 4002 Basel, Switzerland
*Correspondence: elisabetta.traggiai@gmail.com
http://dx.doi.org/10.1016/j.celrep.2013.05.022

SUMMARY

Immunoglobulin (Ig) isotype diversification by class switch recombination (CSR) is an essential process for mounting a protective humoral immune response. Ig CSR deficiencies in humans can result from an intrinsic B cell defect; however, most of these deficiencies are still molecularly undefined and diagnosed as common variable immunodeficiency (CVID). Here, we show that extracellular adenosine critically contributes to CSR in human naive and IgM memory B cells. In these cells, coordinate stimulation of B cell receptor and toll-like receptors results in the release of ATP stored in Ca^{2+}-sensitive secretory vesicles. Plasma membrane ectonucleoside triphosphate diphosphohydrolase 1 CD39 and ecto-5′-nucleotidase CD73 hydrolyze ATP to adenosine, which induces CSR in B cells in an autonomous fashion. Notably, CVID patients with impaired class-switched antibody responses are selectively deficient in CD73 expression in B cells, suggesting that CD73-dependent adenosine generation contributes to the pathogenesis of this disease.

INTRODUCTION

Different cell types, including astrocytes, endothelial cells, platelets, T cells, and monocytes, release ATP in the extracellular space as signaling molecules acting in a paracrine/autocrine fashion (Corriden and Insel, 2010). Thus, transient and regulated increases in extracellular ATP (eATP) are used for basic physiological signaling in the nervous, vascular, and immune systems. On the other hand, extracellular levels of ATP are controlled by the expression of ectonucleotidases in the plasma membrane. The rate-limiting step of the ectonucleotidase cascade for adenosine generation is represented by CD39 (E-NTPDase 1), an ectonucleoside triphosphate diphosphohydrolase that hydrolyzes ATP/UTP and ADP/UDP to the respective nucleoside (e.g., AMP). In turn, extracellular nucleoside monophosphates are rapidly degraded to adenosine by plasma membrane ecto-5′-nucleotidase CD73 (Deaglio and Robson, 2011). More than 40 years ago, reduced CD73 activity was detected in lymphocytes of patients suffering from immunodeficiency syndromes characterized by hypo- and agammaglobulinemia (Johnson et al., 1977; Edwards et al., 1978), but so far no functional relationship between B cell dysfunction and defects in enzymatic activity has been defined.

RESULTS AND DISCUSSION

CD73 was originally used as a surface marker to identify individual B cell subsets at specific stages of differentiation (Resta et al., 1998; Thompson and Ruedi, 1988). CD73 is expressed in a subset of $CD39^+$-naive (59.3% ± 8.1%), memory (60.9% ± 9.3%), and to a lesser extent germinal-center (12.9% ± 5.7%) cells in tonsils and in a subset of $CD39^+$-naive (45.1% ± 7.7%), immunoglobulin M (IgM) memory (21.9% ± 5.4%), and switched memory B (27^+ 50.2% ± 5.1%, 27^- 41.7 ± 8.8) cells in the blood

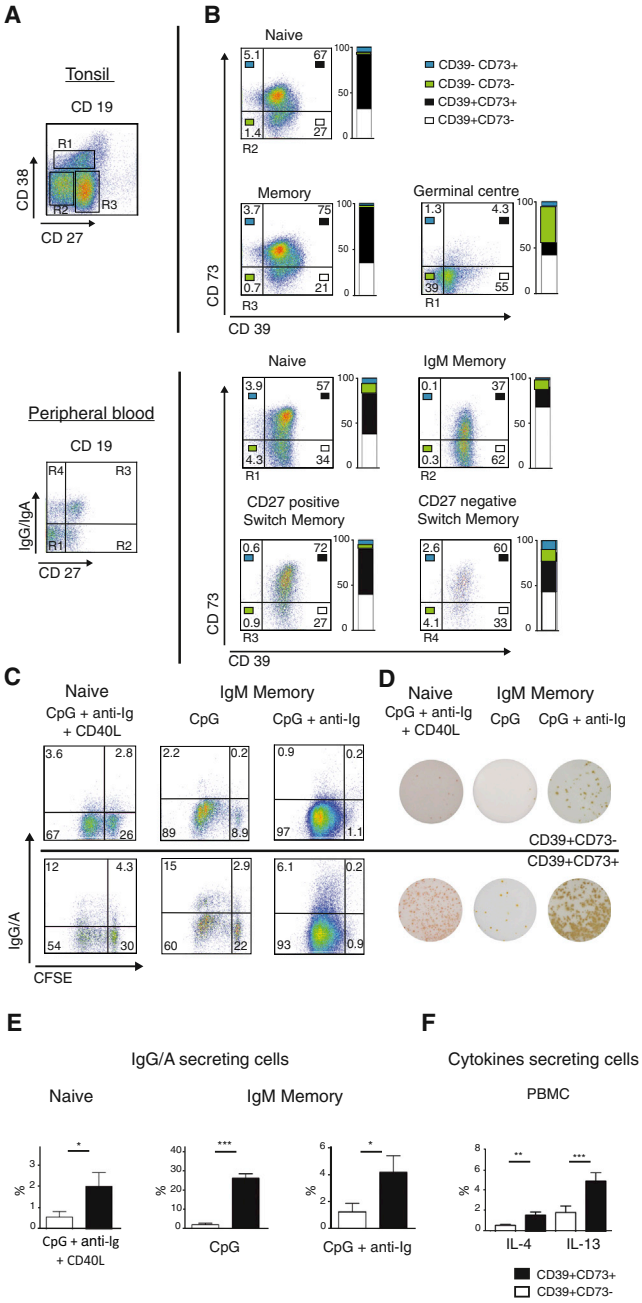

Figure 1. CD39 and CD73 Expression in Human B Cells Correlates with CSR

(A) Human mature B cell subsets in peripheral blood (lower panel) and tonsil (upper panel) were identified by flow cytometry with a combination of monoclonal antibodies specific for CD19, CD27, IgG/IgA and CD19, CD38, and CD27, respectively. Dot plots were electronically gated on CD19$^+$ B cells to identify the following subpopulations: R1, CD19$^+$CD27$^-$IgG/IgA$^-$ naive, R2 CD19$^+$CD27$^+$IgG/IgA$^-$ IgM memory, R3 CD19$^+$CD27$^+$IgG/IgA$^+$ switch memory B cells, R4 CD19$^+$CD27$^-$IgG/IgA$^+$ switch memory B cells in peripheral blood, and R1 CD19$^+$CD38$^+$CD27$^+$ germinal center, R2 CD19$^+$CD38$^-$CD27$^-$ naive, and R3 CD19$^+$CD38$^-$CD27$^+$ memory B cells in tonsil.

(B) Representative analysis of CD39 and CD73 expression in B cell subsets in peripheral blood (upper panels) and tonsil (lower panels). Numbers reported in dot plots indicate the percentage of cells within the quadrant. Bars show mean percentages of B cell subsets in normal donors according to the indicated CD39 and CD73 phenotype; peripheral blood n = 10, tonsil n = 6.

(C) CFSE dilution and expression of surface IgG and IgA in CD39$^+$73$^-$ (upper row) and CD39$^+$73$^+$ (lower row) naive and IgM memory B cells after 6 days stimulation with CpG 2006, anti-ig and CD40L or CpG 2006, or CpG 2006 and anti-Ig, in the presence of IL-2.

(D) Representative pictures of IgG/IgA-secreting cells in ELISPOT assay.

(E) Statistics of IgG/IgA-secreting cells in ELISPOT assay after 6 days of stimulation, expressed as percentage of live cells (open bars: CD39$^+$CD73$^-$, black bars: CD39$^+$CD73$^+$). Left panel: mean + SD, n = 10, *p = 0.0213; middle panel: mean + SD, n = 2–4, **p = 0.000174; right panel: mean + SD, n = 8, *p = 0.032.

(F) Frequency of IL-4- and IL-13-secreting cells in the indicated subsets (open bars: CD39$^+$CD73$^-$; black bars: CD39$^+$CD73$^+$ cells) of CD19$^+$27$^+$ memory B cells after 5 hr stimulation with CpG 2006, anti-Ig, and CD40L. IL-4: n = 9, **p < 0.008; IL-13: n = 9, **p < 0.0001.

(Figures 1A and 1B). A detailed analysis of CD39 and CD73 expression in murine B cell subsets revealed the preferential expression of CD73 in mature class-switched and germinal-center B cells (Figure S1A).

To address whether the ATP-hydrolases CD39 and CD73 contribute to signals leading to B cell activation, we stimulated naive and memory B cells purified on the basis of CD73 expression with anti-B cell receptor (anti-Ig) antibody, CD40L, and CpG 2006 as the toll-like receptor 9 (TLR9) ligand. CD39$^+$CD73$^+$-naive and memory B cells did not display any substantial differences in proliferative activity with respect to CD39$^+$CD73$^-$ B cells (Figure S2A). However, the percentage of naive and IgM memory B cells, which switched in vitro to IgG or IgA, was enriched in the CD39$^+$73$^+$ fraction (Figure 1C). Accordingly, the frequency of IgG or IgA secreting cells (ISCs) as measured by enzyme-linked immunosorbent spot (ELISPOT) assay was significantly higher in CD73$^+$ cells (Figures 1D and 1E). Remarkably, class switch recombination (CSR) in response to TLR9 stimulation was confined within the CD73-expressing IgM memory B cells (Figures 1D and 1E). *Tlr9* was expressed to the same extent in CD39$^+$CD73$^+$ and CD39$^+$CD73$^-$ memory B cells (Figure S3B). Analysis of transcription factors involved in late B cell development, revealed in IgM memory CD39$^+$CD73$^+$ B cell subsets a significant increase in the expression of *Xbp-1* (Figures S3C and S3D). Naive and IgM memory B cell subsets coexpressing CD39 and CD73 were also analyzed for the expression of surface markers involved in T cell costimulation, B cell activation, and survival, and compared with CD39 single-positive B cells. Surface expression of CD180, a TLR homolog that influences the sensitivity of naive as well as memory B cells to stimulation via TLR9 and CD40L (Good et al., 2009), was significantly increased in CD39$^+$CD73$^+$ with respect to CD39-only B cells. In addition, BAFFR and TACI, which belong to the tumor necrosis factor α (TNF-α) family, were increased in both CD39$^+$CD73$^+$-naive and memory B cells (Figure S4). We also evaluated whether mouse naive B cells coexpressing CD39 and CD73 differentiated more efficiently to class-switched ISC with respect to CD39 single-positive naive B cells. The CD39$^+$CD73$^+$ fraction was enriched in cells, which switched in vitro to IgG (LN cells) and to both IgG and IgA (PP cells). Accordingly, the frequency of IgG or IgA ISCs measured by ELISPOT assay was significantly higher in the CD73$^+$ subset (Figure S1B). CSR is induced by interleukin-4 (IL-4) and IL-13

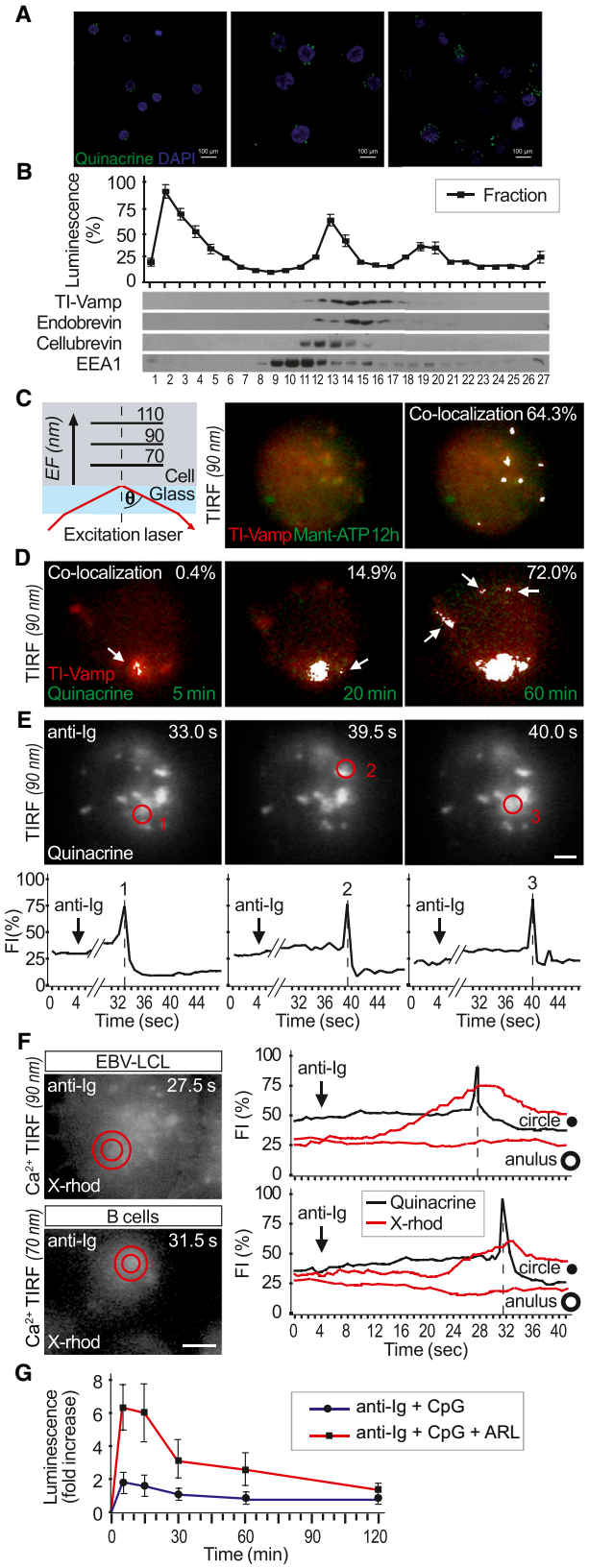

Figure 2. Storage and Release of ATP in Human B Cells

(A) Purified naive (left panel) and memory (middle panel) B cells, and EBV-LCL (right panel) were labeled with quinacrine and DAPI and analyzed by confocal microscopy.

(B) Subcellular fractionation of EBV-LCL on equilibrium sucrose gradient. Luciferase assay for ATP content in each fraction, expressed as percentage of luminescence. Western blot for Ti-VAMP, endobrevin, cellubrevin, and early endosomal marker EEA1 on the isolated fractions.

(C) In dual-wavelength recording by TIRF microscopy, the laser beam was tilted at a precise critical angle (θ) to obtain total internal reflection at the glass-cell interface (left panel). The dynamic scanner (Leica AM TIRF MC) precisely positioned the laser beam and determined the exact penetration depth of the evanescent field (EF). To confine the analysis to juxtamembrane regions of the cells with high spatial resolution, we restricted the excitation and detection of the fluorophores to 70–90 nm in depth. EBV-LCL cells transfected with TI-Vamp RFP were incubated with Mant-ATP for 12 hr. In live experiments, Mant-ATP (green) and TI-Vamp RFP (red) signals were imaged in sequential mode under EF illumination (middle panel). Colocalization signals of the two fluorophores, above background threshold, are shown as a binary image (white) and superimposed onto fluorescent signals (right panel). The contribution of Mant-ATP signal to the colocalization areas is expressed as percentage (Manders' M1 coefficient). A substantial portion of exogenous Mant-ATP co-localized with TI-VAMP RFP in submembrane granules.

(D) EBV-LCL cells transfected with TI-Vamp RFP were incubated with quinacrine at different times (5, 20, and 60 min). Quinacrine loaded into TI-Vamp-positive vesicles is shown as colocalization signals (white) as in (C). Arrows indicate the appearance of the colocalization signals at each investigated time.

(E) Live TIRF imaging of secretory events in EBV-LCL cells incubated with quinacrine for 60 min. Quinacrine displays marked pH dependence and accumulates in a self-quenched state inside acidic vesicles. Exocytosis is revealed by the occurrence of fluorescence dequenching (light flash) caused by the rapid increase in pH upon diffusion of quinacrine to the extracellular medium. Individual secretory events were analyzed in basal conditions and upon stimulation with anti-ig. Graphics below show changes of fluorescence intensity (FI) in selected regions surrounding vesicles exocytosis (red circles, 1–3). Only when quinacrine fluorescence increased and then declined below the basal level was the event counted as a secretory event. To prevent photobleaching and phototoxicity of the sample, TIRF images were acquired for only 40 ms at 250 ms intervals. Light was filtered with dual-band-filter sets and fluorescence images were visualized using a CCD camera. The scale bar represents 1 μm.

(F) Live Ca^{2+} TIRF imaging of secretory events in EBV-LCL (upper panel) and B cells (lower panel) incubated with quinacrine and X-rhod for 60 min. Changes in X-rhod fluorescence intensity, revealing Ca^{2+} levels, were analyzed in regions (circle and concentric annulus) surrounding quinacrine-labeled vesicles in basal conditions and upon stimulation with anti-ig. Graphics on the right show changes of quinacrine and X-rhod fluorescence intensity in the regions of interest. The scale bar represents 1 μm.

(G) ATP content in the supernatants of human B cells stimulated in vitro with CpG 2006 and anti-Ig at different time points by luciferase assay. Measurements were performed with or without ARL, an inhibitor of the ectonucleotidases CD39 and CD73. Mean ± SD, n = 4.

(Dunnick et al., 2011; Iwata et al., 2011), and stimulation of B cells determined an increase in IL-4- and IL-13-secreting cells in the $CD73^{+}$ memory pool (Figure 1F). Interestingly, purinergic receptors, in particular adenosine receptors, were previously shown to stimulate IL-4 secretion in mast cells (Ryzhov et al., 2004). Staining of naive, memory B cells and Epstein-Barr virus immortalized lymphoblastoid cell lines (EBV-LCL) with the fluorescent, nucleotide-binding component quinacrine (Bodin and Burnstock, 2001; Sorensen and Novak, 2001) revealed a punctate staining indicative of ATP-filled vesicles (Figure 2A). Subcellular fractionation of EBV-LCL on sucrose equilibrium gradients revealed, in addition to cytosolic ATP, a purine peak that overlapped with the late endosomal and lysosomal

TI-VAMP/VAMP7, and to a much lesser extent with endobrevin and the early and recycling endosomal cellubrevin, but not with the early endosome marker EEA1 (Figure 2B; Stow et al., 2006; Chaineau et al., 2009). These results indicate that ATP accumulates in late endosomal/lysosomal vesicular compartments in human B cells. TI-VAMP is a vesicular SNARE protein that is involved in lysosomal secretion and was shown to colocalize with ATP in astrocytes (Verderio et al., 2012). In EBV-LCL expressing a TI-VAMP fused to red fluorescent protein (RFP), total internal reflection fluorescence (TIRF) illumination revealed a punctate pattern of TI-VAMP-RFP within submembrane regions, suggesting the secretory nature of these vesicles (Figure 2C). Incubation of EBV-LCL expressing TI-VAMP-RFP with Mant-ATP, a fluorescent nucleotide analog (Zhang et al., 2007), demonstrated colocalization of Mant-ATP$^+$ vesicles with TI-VAMP-RFP$^+$ submembrane puncta. Quinacrine labeling confirmed that ATP-filled vesicles colocalized with TI-VAMP-RFP, with a progressive increase over time (Figure 2D). Monitoring of fluorescence changes in the submembrane compartment of primary human B cells and EBV-LCL labeled with quinacrine upon stimulation with anti-ig by time-lapse TIRF showed the appearance of light flashes in different positions of the plasma membrane at different times (33.0, 39.5, and 40.0 s), indicative of regulated vesicular release (Figure 2E; Movie S1). To directly address the role of TI-VAMP in ATP release by B cells, we used TI-VAMP-deficient mice (Danglot et al., 2012). Murine B cells release ATP with analogous kinetics of human B cells (Figure S5A). However, TI-VAMP-deficient B lymphocytes displayed reduced eATP levels upon stimulation with CpG, anti-Ig, anti-CD40, and IL-21 (see below), and significantly reduced the frequency of IgG and IgA ISC, suggesting that TI-VAMP is involved in ATP release and CSR in B cells (Figures S5B and S5C). To define the stimulus-secretion coupling mechanism, we investigated Ca^{2+} elevation during exocytosis (Figure 2F). Labeling of cells with quinacrine and the Ca^{2+} indicator X-rhod, and imaging under dual-wavelength TIRF before and after anti-Ig stimulation showed Ca^{2+} events restricted to individual vesicles (circle) and the surroundings of the fusion event (anulus). The submembrane Ca^{2+} ions were increased in strict spatial correlation with the sites of vesicular fusion without lateral propagation of the signal. The decrease of submembrane Ca^{2+} events once exocytosis was completed, as compared with intracellular Ca^{2+} in widefield imaging (Figures S2B and S2C), suggests that subplasma membrane Ca^{2+} rises around the vesicular organelle for the time required for exocytosis. This observation directly proves that fast submembrane Ca^{2+} elevations are the events that trigger ATP secretion in human B lymphocytes. Stimulation of human B cells by anti-Ig and CpG led to ATP release in the culture supernatant (Figure 2G). This increase was augmented up to 6-fold by ARL67156, an efficient inhibitor of NTPDase1 and a partially effective inhibitor of CD73 (Lévesque et al., 2007; Karczewska et al., 2007), suggesting that CD39 and CD73 were actively hydrolyzing the ATP that was released upon cell stimulation. Thus, we measured adenosine in culture medium at 40 min after addition of exogenous ATP. Naive and memory CD73$^+$ B lymphocytes generated substantially more adenosine than the CD73$^-$ counterpart (Figure 3A). Treatment of CD73$^+$ cells with ARL67156 or a,b-methylene ADP (APCP), a specific CD73 inhibitor, blocked adenosine generation and resulted in accumulation of ATP and AMP, respectively (Figure 3A). The generation of adenosine by CD73$^+$ cells results in stimulation of A_{2A} adenosine receptor subtype, which is expressed in B cells (Junger, 2011) (Figure S3A). To determine whether extracellular adenosine plays a role in CSR, we treated stimulated naive and memory CD73$^+$ B cells with ARL67156 and adenosine deaminase (ADA), which degrades adenosine to inosine (Sauer and Aiuti, 2009). Both treatments significantly affected the generation of isotype switched immunoglobulin of both naive and IgM memory B cells (Figure 3B). To directly address the role of adenosine in Ig isotype switching, we incubated naive and memory cells with adenosine in combination with anti-Ig, CpG 2006, and CD40L. Adenosine significantly increased the differentiation of naive and memory CD73$^-$ B cells to class-switched B cells (Figure 3B). These results suggest that adenosine generated by the sequential activity of CD39 and CD73 on endogenous ATP released upon B cell stimulation significantly contributes to CSR. Remarkably, no differences in adenosine receptor expression were observed in CD39$^+$CD73$^+$ naive and memory B cells compared with CD39$^+$CD73$^-$ B subsets (Figure S3A). To directly test the role of CD73 in CSR, we purified naive B cells from LNs and PPs of *Nt5e* (CD73)-deficient mice. IL-21 induces CD73 expression in mouse Th17 lymphocytes (Chalmin et al., 2012), and we observed the same effect in mouse naive B cells (Figures S6A and S6B). Stimulation of naive B cells isolated from LNs and PPs of *Nt5e*$^{-/-}$ mice displayed a significant impairment in their capacity to differentiate into class-switched IgG ISC after in vitro stimulation with CpG and IL-21 or CpG, anti-Ig, and IL-21 (Figure S6C). We then addressed whether expression of CD73 and CD39 was altered in a cohort of patients with common variable immunodeficiency (CVID). CVID is the most common clinically significant primary B cell immune deficiency and is characterized by hypogammaglobulinemia, increased susceptibility to infections, and autoimmune manifestations (Eibel et al., 2010). Patients with CVID display reduced percentages of switched memory B cells expressing IgG and IgA, and impaired capacity to respond to antigen-dependent vaccination (Chovancova et al., 2011; Foerster et al., 2010; van de Ven et al., 2011). Remarkably, a significant decrease in cell-surface expression of CD73 was observed in naive, IgM memory, and switched memory B cells of CVID patients compared with age-matched controls (measured as the mean fluorescence intensity as well as the percentage of CD73-expressing cells), whereas CD39 expression was comparable in all B cell subsets (Figures 4 and S7). CD73 was undetectable by intracellular staining, indicating that the absence of CD73 in the plasma membrane was not due to a defect in the secretory pathway (Figure S8B). We then induced CSR in vitro in CD19$^+$ B cells by anti-Ig, bystander T cell help, and CpG 2006. Although these culture conditions promoted CSR in B cells from normal donors, they were completely ineffective in B cells from a CVID patient with defective CD73 expression (Figures S8C and S8D). In contrast to control cells, CVID B cells failed to upregulate activation-induced cytidine deaminase (AID) and BCL6, which were both strongly transcribed in activated B cells from healthy donors (Figure S8E). Because in addition to CSR, AID promotes somatic hypermutation of Ig variable region genes, we analyzed VDJ

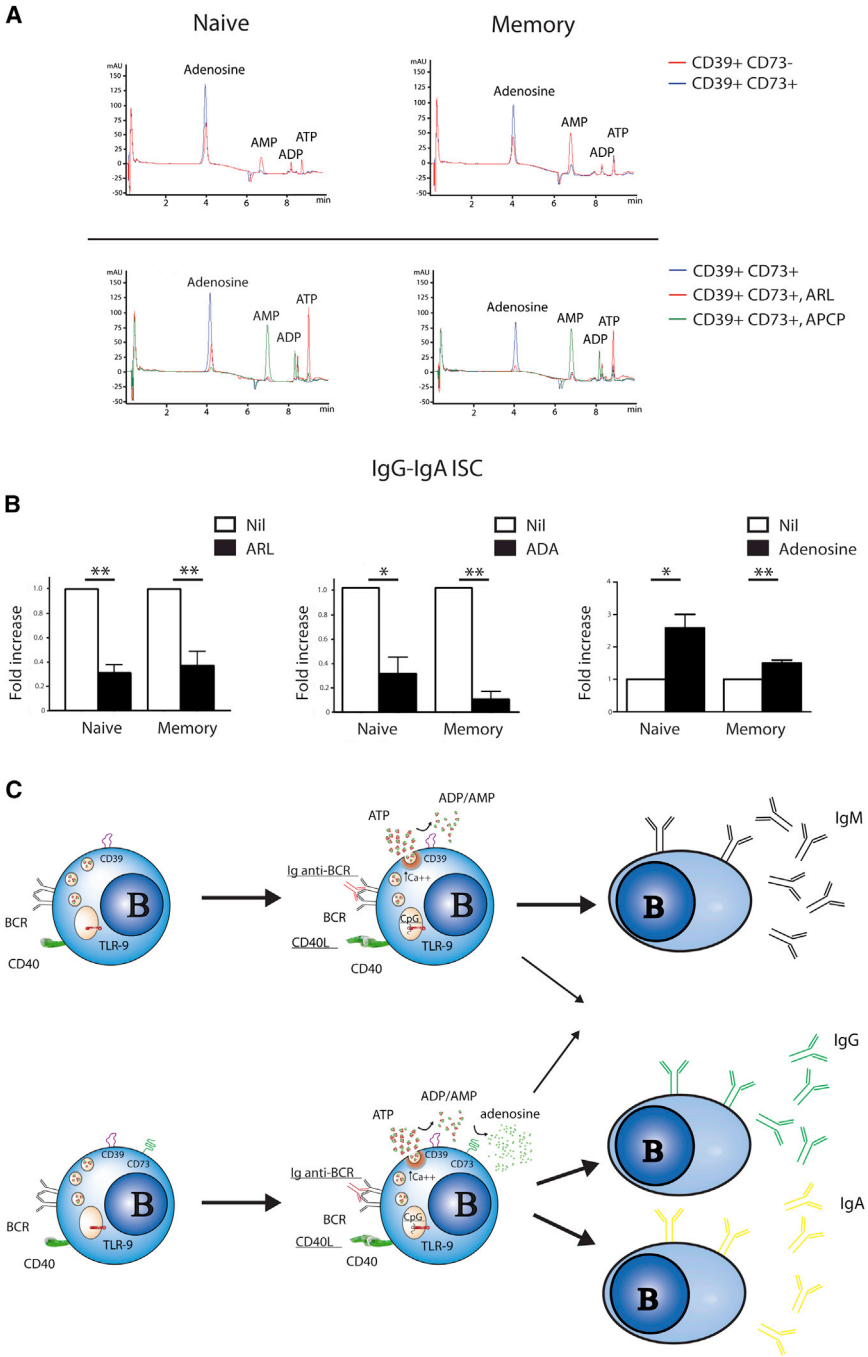

Figure 3. Adenosine Generation in CSR

(A) Upper panel: HPLC analysis of ATP, ADP, AMP, and adenosine content in the supernatants of purified $CD39^{+}CD73^{-}$ and $CD39^{+}CD73^{+}$ naive and IgM memory B cells after addition of exogenous ATP. Lower panel: The same analysis was performed in the presence of ectonucleotidase inhibitor ARL (red line) and the CD73 inhibitor APCP (green line). One representative experiment out of four is shown.

(B) Fold increase of IgG/IgA-secreting cells in ELISPOT assay on purified naive and memory B cells after 6 days of stimulation with CpG 2006/anti-ig/CD40L and CpG 2006/anti-ig, respectively, with or without ARL (100 μM; n = 4–5, **p = 0.0016, **p = 0.0052), ADA (50 μM; n = 3–4, *p = 0.012, **p = 0.0043), and adenosine (10 μM; n = 4–6, *p = 0.03, **p = 0.004).

(C) Schematic representation of the hypothesized role played by CD73/adenosine in CSR in B cells.

rearrangements and mutations in B cells from one CVID patient. Whereas the rate of mutations in healthy donors was 5.3 per B cell clone, an analysis of 75 individual B cell clones from the CVID donor revealed a total of 83 somatic mutations corresponding to 1.27 mutations per clone (Figure S8A). These results indicate that AID is less active in stimulated B cells from CVID patients and this decrease in activity correlates with lack of CD73. Restoration of AID activity and CSR in B cells from CVID patients by stimulation with adenosine might be limited by the coordinate regulation of CD73 and adenosine receptor responsiveness in human B cells (Napieralski et al., 2003). Altogether, these data show that in human B cells, ATP is stored in secretory vesicles that are released in a Ca^{2+}-sensitive fashion upon BCR stimulation. We propose that CD73-dependent adenosine generation favors CSR, endowing the B cell with an intrinsic control of differentiation toward Ig class-switched plasma cells.

EXPERIMENTAL PROCEDURES

Blood Samples and Patients

Blood samples from healthy donors and 24 CVID patients were obtained from the Hospital Gaslini Institute and the Centre of Chronic Immunodeficiency, University Medical Centre. Informed written consent was obtained from each individual before participation, with approval from the internal ethics review board (239/99 and 78/2001).

Media and Reagents for B Cell Culture

The medium used for B cell culture was RPMI 1640 (BioWhittaker) supplemented with 10% fetal bovine serum (Defined; Hyclone) 2 mM GlutaMAX (GIBCO), 10 mg/ml nonessential amino acids, 1 mM pyruvate, 50 U/ml penicillin, 50 U/ml streptomycin, 50 U/ml kanamycin (GIBCO), and 5×10^{-2} M 2-mercaptoethanol (Sigma-Aldrich). The following chemical compounds were used in the B cell culture system: ARL (100 μM), adenosine deaminase (50 μM), and adenosine (10 μM) (Sigma-Aldrich).

Isolation of Human B Cell Subsets and Flow Cytometry Analysis

Peripheral blood mononuclear cells (PBMCs) were isolated by Ficoll-Hypaque density centrifugation and stained with the following monoclonal antibodies: CD19, CD73 (Becton Dickinson), CD27, CD39 (eBioscience), and surface IgG and IgA (Jackson ImmunoResearch Laboratories). To perform functional assays, $CD19^{+}$ B cells were isolated with CD19 microbeads (Miltenyi Biotec)

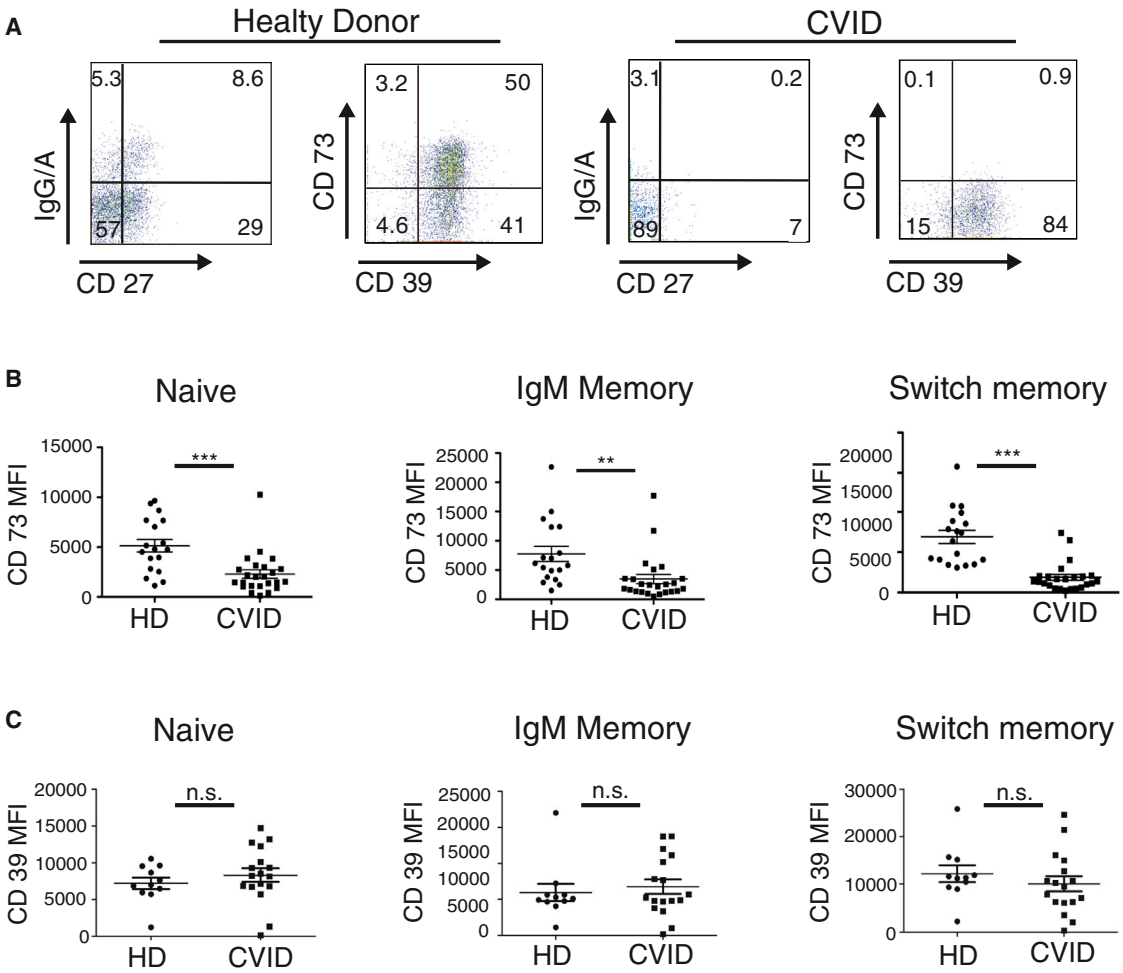

Figure 4. Selective CD73 Defect in B Cells from CVID Patients

(A) Flow cytometry for IgG/IgA, CD27 and CD39, and CD73 expression in electronically gated CD19$^+$ B cells from a representative CVID patient and an age-matched healthy donor.

(B) Mean fluorescent intensity (MFI) of CD73 in naive, IgM memory, and switched memory B cells in CVID patients compared with age-matched controls (n = 11–17, ***p = 0.0004, **p = 0.005, ***p < 0.0001).

(C) MFI of CD39 in naive, IgM memory, and switched memory B cells in CVID patients compared with age-matched controls (n = 11–23).

according to the manufacturer's instructions. Following staining for lineage (CD3, CD14, and CD56; Beckman Coulter), CD19, CD27, surface IgG and IgA, CD39, CD73, and naive and IgM memory B cells were sorted according to the expression of CD73 and CD39 with the use of a cell sorter (FACSAria).

Murine B Cell Isolation and Flow Cytometry

Naive B lymphocytes were isolated from LNs of wild-type (WT), *Vamp7*$^{-/-}$, and *Nt5e*$^{-/-}$ mice by negative enrichment with CD43 beads, followed by staining for the lineage markers CD19, B220, IgG, and IgA, and then isolated by cell sorting as CD19$^+$ B220$^+$ IgG$^-$IgA$^-$. PP B cells from WT, *Vamp7*$^{-/-}$, and *Nt5e*$^{-/-}$ mice were directly stained with monoclonal antibodies specific for CD19, B220, IgG, and IgA, and isolated as CD19$^+$ B220$^+$ IgG$^-$IgA$^-$.

Human and Murine Proliferation Assay

Human B cell subsets were labeled with 0.5 μM 5-(and-6-)-carboxyfluorescein diacetate, succinimidyl ester (CFSE) (Molecular Probes) for 8 min at room temperature. Purified B cells (2–5 × 10^4 cells) were activated in 96-well flat-bottom plates with the following stimuli: (1) 2.5 μg/ml CpG oligodeoxynucleotide 2006 (5′-tcgtcgttttgtcgttttgtcgtt-3′; TIB Molbiol), (2) 2.5 μg/ml F(ab′)$_2$ anti-human IgM/IgA/IgG (Jackson ImmunoResearch Laboratories), (3) megaCD40L 12 ng/ml (Alexis), and (4) 2000 U/ml IL-2 (Proleukin; Chiron). The proliferation profile of propidium-iodide-negative viable CD19-positive cells was analyzed at day 4 of culture. To allow a direct quantitative comparison of B cell proliferation in the different conditions, fluorescence-activated cell sorting (FACS) acquisitions were standardized by a fixed number of calibration beads (BD Biosciences). Purified murine B lymphocytes were labeled with CellTracker Violet (Molecular Probes) and stimulated in vitro in 96-well flat-bottom plates with (1) 2.5 μg/ml CpG oligodeoxinucleotides 1826 (5′-tccatgacgttcctga cgtt-3′; Microsynth), (2) 2.5 μg/ml anti-Ig M (Jackson ImmunoResearch Laboratories), (3) 10 ng/ml or 20 ng/ml of IL-21 (for PP and LN, respectively; R&D Systems), and (4) IL-2 100 UI/ml (Proleukin; Chiron).

ELISPOT

Plasma cells secreting IgG, IgM, or IgA were detected using an ELISPOT assay. Briefly, 96-well plates (Millipore; Billerica) were coated with 10 μg/ml purified goat anti-human IgG or IgA or IgM (Southern Biotechnologies). After washing and blocking with 1% BSA in PBS for 30 min, serial dilutions of cultured B cells were added and incubated overnight at 37°C. The plates

were washed and incubated with isotype-specific, biotin-conjugated secondary antibodies, followed by streptavidin-HRP (Sigma-Aldrich). The assay was developed with AEC (Sigma-Aldrich).

Intracellular Cytokine Secretion Analysis of Human B Cell Subsets

Peripheral B cells were enriched from PBMCs from healthy donors with CD20 microbeads (Miltenyi). B cells were cultured with the following stimuli: Cpg (2.5 μg/ml), anti-Ig (2.5 ug/ml), IL2 (2000 U/ml), megaCD40L (12 ng/ml), BFA (10 μg/ml), ionomycin (1 μg/ml), and phorbol 12-myristate 13-acetate (PMA; 50 ng/ml) for 5 hr (all from Sigma-Aldrich). Cells were stained for cell-surface CD19, CD27, CD39, and CD73, and cytoplasmic expression of IL-4 or IL-13 according to the intracellular staining protocol for the Cytofix/Cytoperm kit (BD Bisciences).

Subcellular Fractionation and Immunoblotting

EBV-B cell line were diluted 1:4 in homogenization buffer (10 mM HEPES-KOH, pH 7.4, 250 mM sucrose, 1 mM Mg acetate, 0.5 mM phenylmethylsulfonyl fluoride, 2 μg/ml pepstatin, 10 μg/ml aprotinin). The cells were homogenized using a cell cracker (European Molecular Biology Laboratory) and centrifuged at 1,000 × *g* for 10 min to prepare the postnuclear supernatant. The supernatant was loaded onto 0.4–1.8 M sucrose gradient and spun in a 41 SW rotor (Beckman Instruments) at 25,000 rpm for 18 hr. Fractions (1 ml) were collected and analyzed by SDS-PAGE followed by western blotting.

Bioluminescence Assay to Measure ATP

For ATP measurement, CD19-positive human B cells were isolated from buffy coats of healthy donors and stimulated in vitro with 2.5 μg/ml CpG 2006 and 2.5 μg/ml $F(ab')_2$ anti-human IgM/IgA/IgG with or without 100 μM ARL, at 10^5 cells/well in 96-well round-bottom plates with a transwell on top. Supernatants of the cell culture were measured using a luciferin/luciferase assay (Molecular Probes) according to the manufacturer's instruction.

High-Performance Liquid Chromatography Analysis of ATP, ADP, AMP, and Adenosine in Human Primary B Cell Culture

To evaluate CD39 and CD73 enzymatic activity, B lymphocytes were isolated by CD19 microbeads. Cells were then diluted in Hank's solution (Sigma-Aldrich) and plated at 10^5 cells/well in 96-well flat-bottom plates in the presence of the following stimuli: ATP (5 μM), ARL (100 μM), and CD73 inhibitor (50 μM). At 0 and 40 min after stimulation, cells were collected and centrifuged. Supernatants were then collected and stored at −80°C. Separation of adenosine and its adenylic nucleotides (AMP, ADP, and ATP) was carried out by reverse-phase high-performance liquid chromatography (HPLC) on an Agilent 1100 Series (Agilent Technologies), using an original method exploiting a Kinetex C18 stationary phase (Phenomenex-Italia).

Time-Lapse TIRF Imaging

To measure vesicle localization, EBV-LCL cells were transfected using the Amaxa Nucleofector technology, with complementary DNA plasmid encoding for TI-VAMP-RFP and coincubated with mant-ATP for 12 hr or quinacrine for a maximum of 60 min. To measure vesicle exocytosis, untransfected cells were loaded with quinacrine for 60 min. To measure submembrane calcium, cells were loaded with quinacrine and X-rhod for 60 min. Time-lapse imaging was conducted using a Leica inverted microscope equipped with a ×60 objective Plapon/TIRFM-SP1 oil immersion and diode solid-state lasers (488 and 532 nm). The laser beam was tilted at a specific critical angle to obtain total internal reflection at the glass-cell interface according to Snell's law. Quinacrine was measured together with TI-VAMP-RFP or X-rhod fluorescence in sequential mode under evanescent field illumination. Fluorescence was measured in circular areas located in the soma and plotted with time.

Statistical Analysis

Unpaired Student's t test was used for statistical comparisons, and p values $\leq$ 0.05 were considered significant.

SUPPLEMENTAL INFORMATION

Supplemental Information includes eight figures and one movie and can be found with this article online at http://dx.doi.org/10.1016/j.celrep.2013.05.022.

LICENSING INFORMATION

This is an open-access article distributed under the terms of the Creative Commons Attribution-NonCommercial-No Derivative Works License, which permits non-commercial use, distribution, and reproduction in any medium, provided the original author and source are credited.

ACKNOWLEDGMENTS

We thank Lydia Danglot for help with the *Vamp7*-deficient mice. We especially thank Lisa Perruzza for crucial support with the *Vamp7*-deficient mice experiments and Emanuela Caci for support and help with the real-time PCR data and analysis. F.G. is supported by the Swiss National Science Foundation (grant 310030-140963). M.R., H.E., and K.W. are supported by BMBF grant CCI-01 EO 0803. M. Rakhmanov is supported by grants from the Forschungskommission and Wissenschaftliche Gesellschaft of the University of Freiburg. E.T. designed the study. F.S., S.V., C.E.F., and E.T. performed most of the experiments. F.P. performed in vitro functional assays. M.P. provided confocal microscopy. U.S. performed cell fractionation in sucrose gradient. S.S. and M.C. performed and designed TIRF experiments and calcium imaging. M.C. contributed with financial support for the acquisition of the TIRF experiment. G.D.M., A.S., and M.B. performed HPLC. T.G. provided reagents and mice. F.F. and C.T. analyzed VDJ rearrangements and somatic hypermutations. A.M. and M.G. contributed with patient samples and financial support. H.E., M. Rizzi, and K.W. contributed with CVID samples and phenotypes. M.I., C.K.A., and M. Rakhmanov provided mice and analyzed adenosine receptor expression in CVID patients. F.S., S.V., M.C., E.T., and F.G. analyzed and revised all of the data. S.V. and S.S. assembled the figures. E.T. and F.G. wrote the paper with the contribution of M.C. regarding the TIRF method.

Received: July 29, 2012
Revised: April 3, 2013
Accepted: May 10, 2013
Published: June 13, 2013

REFERENCES

Bodin, P., and Burnstock, G. (2001). Evidence that release of adenosine triphosphate from endothelial cells during increased shear stress is vesicular. J. Cardiovasc. Pharmacol. *38*, 900–908.

Chaineau, M., Danglot, L., and Galli, T. (2009). Multiple roles of the vesicular-SNARE TI-VAMP in post-Golgi and endosomal trafficking. FEBS Lett. *583*, 3817–3826.

Chalmin, F., Mignot, G., Bruchard, M., Chevriaux, A., Végran, F., Hichami, A., Ladoire, S., Derangère, V., Vincent, J., Masson, D., et al. (2012). Stat3 and Gfi-1 transcription factors control Th17 cell immunosuppressive activity via the regulation of ectonucleotidase expression. Immunity *36*, 362–373.

Chovancova, Z., Vlkova, M., Litzman, J., Lokaj, J., and Thon, V. (2011). Antibody forming cells and plasmablasts in peripheral blood in CVID patients after vaccination. Vaccine *29*, 4142–4150.

Corriden, R., and Insel, P.A. (2010). Basal release of ATP: an autocrine-paracrine mechanism for cell regulation. Sci. Signal. *3*, re1.

Danglot, L., Zylbersztejn, K., Petkovic, M., Gauberti, M., Meziane, H., Combe, R., Champy, M.F., Birling, M.C., Pavlovic, G., Bizot, J.C., et al. (2012). Absence of TI-VAMP/Vamp7 leads to increased anxiety in mice. J. Neurosci. *32*, 1962–1968.

Deaglio, S., and Robson, S.C. (2011). Ectonucleotidases as regulators of purinergic signaling in thrombosis, inflammation, and immunity. Adv. Pharmacol. *61*, 301–332.

Dunnick, W.A., Shi, J., Holden, V., Fontaine, C., and Collins, J.T. (2011). The role of germline promoters and I exons in cytokine-induced gene-specific class switch recombination. J. Immunol. *186*, 350–358.

Edwards, N.L., Magilavy, D.B., Cassidy, J.T., and Fox, I.H. (1978). Lymphocyte ecto-5′-nucleotidase deficiency in agammaglobulinemia. Science *201*, 628–630.

Eibel, H., Salzer, U., and Warnatz, K. (2010). Common variable immunodeficiency at the end of a prospering decade: towards novel gene defects and beyond. Curr. Opin. Allergy Clin. Immunol. *10*, 526–533.

Foerster, C., Voelxen, N., Rakhmanov, M., Keller, B., Gutenberger, S., Goldacker, S., Thiel, J., Feske, S., Peter, H.H., and Warnatz, K. (2010). B cell receptor-mediated calcium signaling is impaired in B lymphocytes of type Ia patients with common variable immunodeficiency. J. Immunol. *184*, 7305–7313.

Good, K.L., Avery, D.T., and Tangye, S.G. (2009). Resting human memory B cells are intrinsically programmed for enhanced survival and responsiveness to diverse stimuli compared to naive B cells. J. Immunol. *182*, 890–901.

Iwata, Y., Matsushita, T., Horikawa, M., Dilillo, D.J., Yanaba, K., Venturi, G.M., Szabolcs, P.M., Bernstein, S.H., Magro, C.M., Williams, A.D., et al. (2011). Characterization of a rare IL-10-competent B-cell subset in humans that parallels mouse regulatory B10 cells. Blood *117*, 530–541.

Johnson, S.M., North, M.E., Asherson, G.L., Allsop, J., Watts, R.W., and Webster, A.D. (1977). Lymphocyte purine 5′-nucleotidase edficiency in primary hypogammaglobulinaemia. Lancet *1*, 168–170.

Junger, W.G. (2011). Immune cell regulation by autocrine purinergic signalling. Nat. Rev. Immunol. *11*, 201–212.

Karczewska, J., Martyniec, L., Dzierzko, G., Stepiński, J., and Angielski, S. (2007). The relationship between constitutive ATP release and its extracellular metabolism in isolated rat kidney glomeruli. J. Physiol. Pharmacol. *58*, 321–333.

Lévesque, S.A., Lavoie, E.G., Lecka, J., Bigonnesse, F., and Sévigny, J. (2007). Specificity of the ecto-ATPase inhibitor ARL 67156 on human and mouse ectonucleotidases. Br. J. Pharmacol. *152*, 141–150.

Napieralski, R., Kempkes, B., and Gutensohn, W. (2003). Evidence for coordinated induction and repression of ecto-5′-nucleotidase (CD73) and the A2a adenosine receptor in a human B cell line. Biol. Chem. *384*, 483–487.

Resta, R., Yamashita, Y., and Thompson, L.F. (1998). Ecto-enzyme and signaling functions of lymphocyte CD73. Immunol. Rev. *161*, 95–109.

Ryzhov, S., Goldstein, A.E., Matafonov, A., Zeng, D., Biaggioni, I., and Feoktistov, I. (2004). Adenosine-activated mast cells induce IgE synthesis by B lymphocytes: an A2B-mediated process involving Th2 cytokines IL-4 and IL-13 with implications for asthma. J. Immunol. *172*, 7726–7733.

Sauer, A.V., and Aiuti, A. (2009). New insights into the pathogenesis of adenosine deaminase-severe combined immunodeficiency and progress in gene therapy. Curr. Opin. Allergy Clin. Immunol. *9*, 496–502.

Sorensen, C.E., and Novak, I. (2001). Visualization of ATP release in pancreatic acini in response to cholinergic stimulus. Use of fluorescent probes and confocal microscopy. J. Biol. Chem. *276*, 32925–32932.

Stow, J.L., Manderson, A.P., and Murray, R.Z. (2006). SNAREing immunity: the role of SNAREs in the immune system. Nat. Rev. Immunol. *6*, 919–929.

Thompson, L.F., and Ruedi, J.M. (1988). Synthesis of immunoglobulin G by pokeweed mitogen- or Epstein-Barr virus-stimulated human B cells in vitro is restricted to the ecto-5′-nucleotidase positive subset. J. Clin. Invest. *82*, 902–905.

van de Ven, A.A., Compeer, E.B., van Montfrans, J.M., and Boes, M. (2011). B-cell defects in common variable immunodeficiency: BCR signaling, protein clustering and hardwired gene mutations. Crit. Rev. Immunol. *31*, 85–98.

Verderio, C., Cagnoli, C., Bergami, M., Francolini, M., Schenk, U., Colombo, A., Riganti, L., Frassoni, C., Zuccaro, E., Danglot, L., et al. (2012). TI-VAMP/VAMP7 is the SNARE of secretory lysosomes contributing to ATP secretion from astrocytes. Biol. Cell *104*, 213–228.

Zhang, Z., Chen, G., Zhou, W., Song, A., Xu, T., Luo, Q., Wang, W., Gu, X.S., and Duan, S. (2007). Regulated ATP release from astrocytes through lysosome exocytosis. Nat. Cell Biol. *9*, 945–953.

Cell PRESS
Open ACCESS

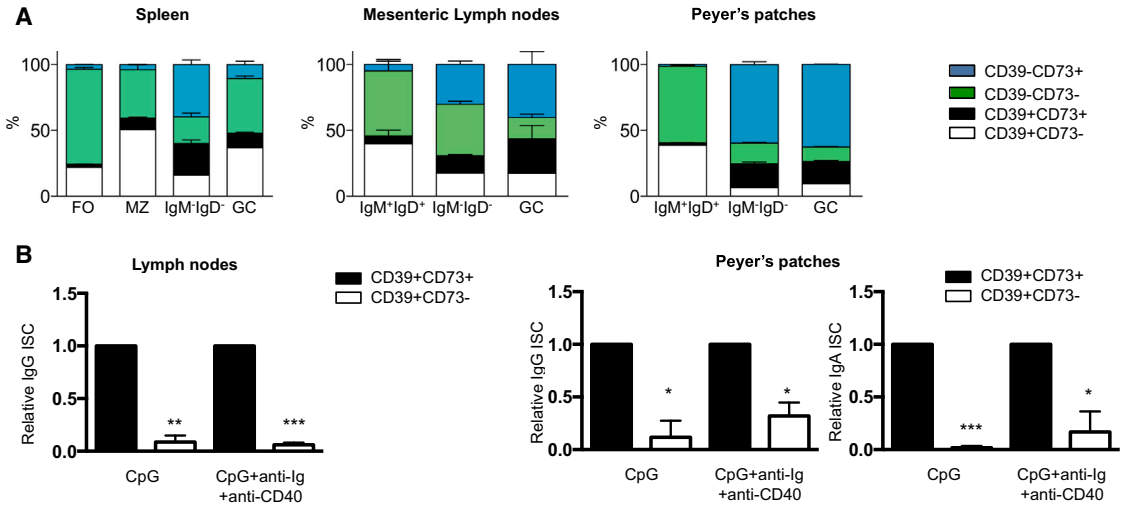

Figure S1. Expression of CD39 and CD73 in Mouse B Lymphocytes and Their Functional Characterization, Related to Results and Discussion

(A) CD39 and CD73 expression in mouse B lymphocyte subsets identified as follows: marginal zone B cells (MZ, $CD19^+B220^+CD21^+CD23^-$), follicular B cells (FO, $CD19^+B220^+CD21^+CD23^+$), isotype switch B cells ($CD19^+B220^+IgM^-IgD^-$) and germinal center B cells (GC, $CD19^+B220^+Fas^+PNA^+$) in the spleen, and naive B cells ($CD19^+B220^+IgM^+IgD^+$), isotype switch B cells ($CD19^+B220^+IgM^-IgD^-$) and germinal center B cells (GC, $CD19^+B220^+Fas^+PNA^+$) in mLNs and PPs. CD73 is expressed in a subset of $CD39^+$ follicular (2.2% ± 0.3), marginal zone (8.6% ± 1.6) B cells, and in a larger fraction of $CD39^+$ isotype switch B cells (24% ± 6.1) and germinal center B cells (11.3% ± 1.6) in the spleen. In mLNs CD73 is expressed in a small subsets of $CD39^+$ mature naive B cells (1.6% ± 0.4) as well as in PPs (1.9% ± 0.3). Remarkably, CD73 is more expressed in isotype switch B cells and GC B cells in mLNs (13% ± 1.8 and 26 ± 2.4 respectively) as well as in PPs (18.1 ± 3.1 and 16.9 ± 1.5, respectively), indicating that CD73 expression is mainly confined to antigen experienced B cell subsets. Bars show distribution of cells in the indicated subset according to CD39 and CD73 expression, spleen, n = 5, LNs, n = 5 and PPs, n = 5.

(B) Naive nonswitch B cells ($CD19^+B220^+IgG^-IgA^-$) from LNs and PPs were sorted as $CD39^+CD73^-$ and $CD39^+CD73^+$ B cells and then stimulated in vitro. Frequency of IgG and IgA secreting cells measured by ELISPOT assay at day 4 after stimulation (LNs IgG ISC, CpG **p = 0.023, CpG, anti-Ig, anti-CD40 ***p = 0.0002; PPs IgG ISC, CpG *p = 0.0155, CpG, anti-Ig, anti-CD40 *p = 0.0172; PPs IgA ISC, CpG ***p = 0.0001, CpG, anti-Ig, anti-CD40 *p = 0.03).

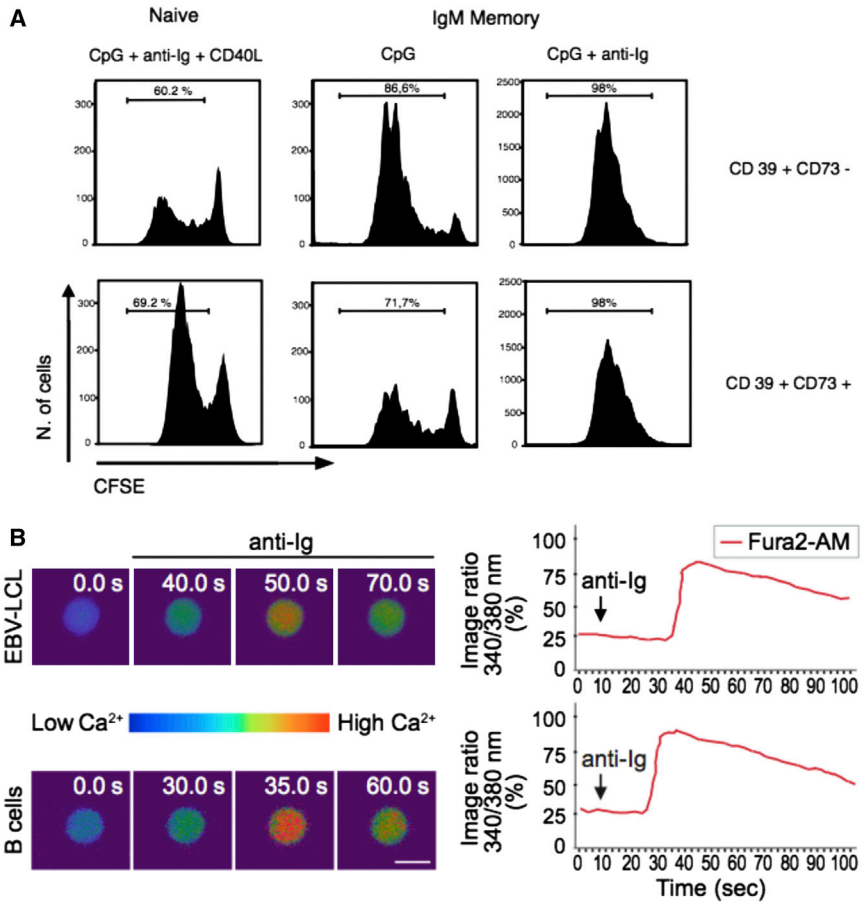

Figure S2. Human B Cell Proliferation of B Lymphocytes and Ca^{2+} Analysis, Related to Results and Discussion

(A) CFSE dilution in $CD39^{+}CD73^{-}$ and $CD39^{+}CD73^{+}$ naive and IgM memory B cells from healthy donors stimulated as indicated. Percentages of cycling cells are shown.

(B) Wide-field Ca^{2+}imaging. Isolated EBV-LCL (upper panels) and B cells (lower panels) were loaded with fura-2 for digital calcium imaging. Fluorochrome excitation (340 and 380 nm) was achieved using a Xenon lamp in series with a filter wile. Emitted light was collected behind a band-pass filter by intensified CCD camera. Images display the spatio-temporal changes of intracellular Ca^{2+} levels. Whole cell Ca^{2+} signal was measured before and after anti-ig stimulation as indicated in the right graphics. Bar, 5 μm.

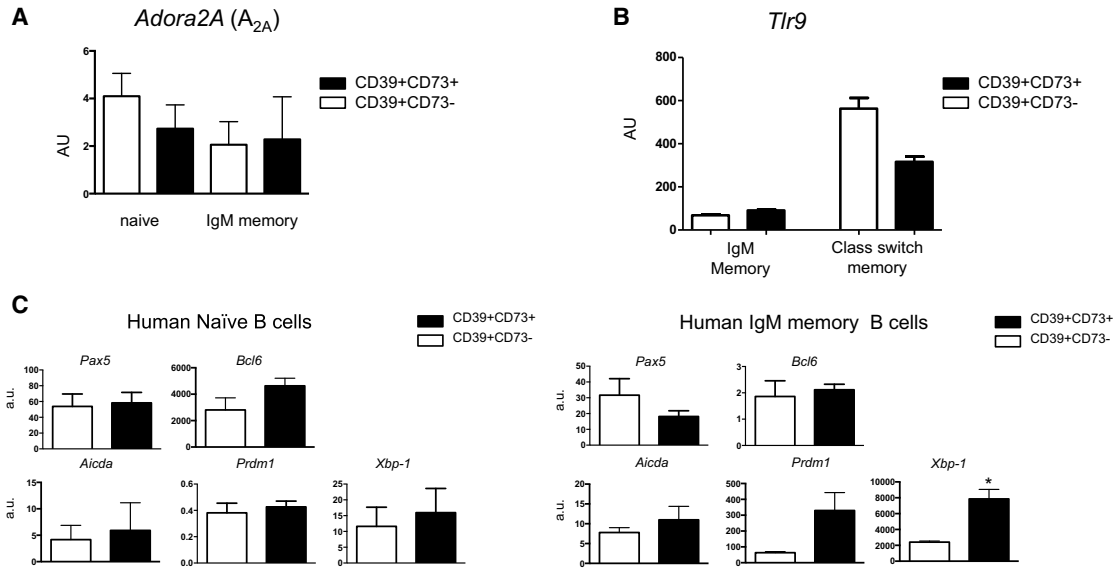

Figure S3. Characterization of Gene Expression in Human B Cell Subsets Isolated According to the Expression of CD39 and CD73, Related to Results and Discussion

(A) *ADORA2A* expression was evaluated in resting $CD39^{+}CD73^{-}$ and $CD39^{+}CD73^{+}$ naive as well as IgM memory B cells (n = 4).

(B) *Tlr9* expression was measured in resting $CD39^{+}CD73^{-}$ and $CD39^{+}CD73^{+}$ IgM memory B cells as well as class switch memory B cells (n = 4).

(C) Expression by RT-PCR of transcription factors involved in late B cell differentiation in resting naive and IgM memory B cells isolated according to the expression of CD39 and CD73 (*PAX5*, n = 4; *BCL6*, n = 2-3, AICDA, n = 3-6, *PRDM1*, n = 2-3, *XBP-1*, n = 3 *p = 0.0470).

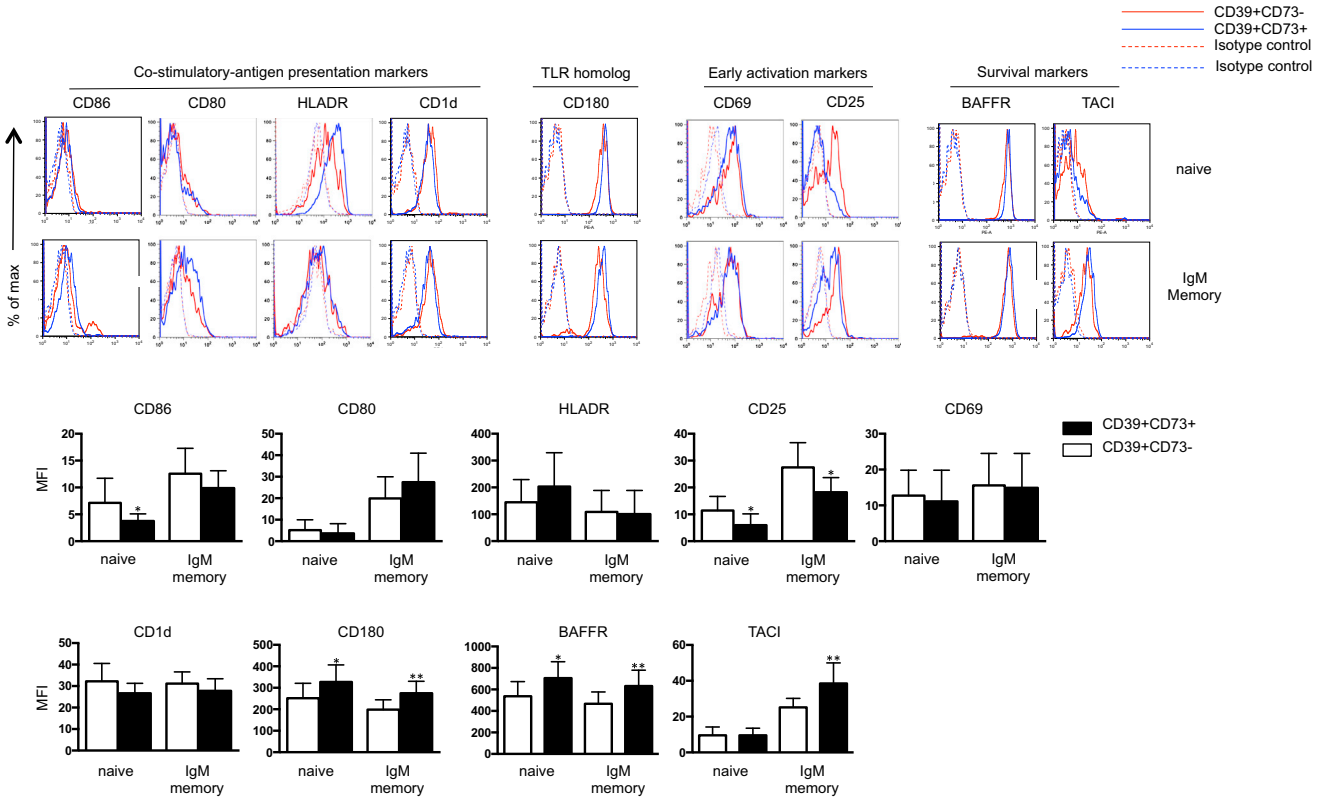

Figure S4. Analysis of Surface Markers Expressed by Human B Cells Isolated According to the Expression of CD39 and CD73, Related to Results and Discussion

Expression of costimulatory surface markers (CD80, CD86, HLADR, CD1d), TLR homolog RP105 (CD180), early activation markers (CD25, CD69) and survival receptors (BAFFR, TACI) on naive and IgM memory B cells subsets identified by staining with mab to CD19, CD27, IgG and IgA in combination twith the specific antibodies and isotype controls (n = 9-10, CD25 on naive *p = 0.0190 and on memory *p = 0.0135; CD180 on naive *p = 0.027 and on memory **p = 0.0023; BAFFR on naive *p = 0.013 and on memory **p = 0.076; TACI on memory **p = 0.0021).

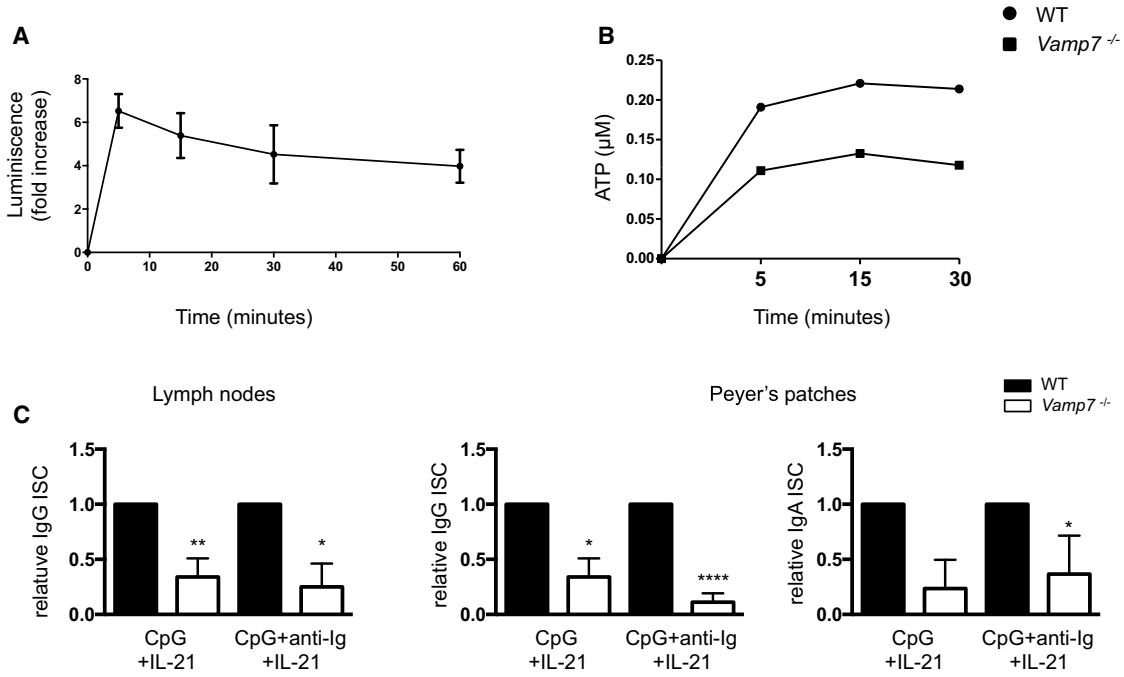

Figure S5. Analysis of ATP Release and Class Switch Recombination in TI-VAMP-Deficient Mouse B Lymphocytes, Related to Results and Discussion

(A) Increase in ATP release from mouse B lymphocytes isolated from WT LNs after in vitro stimulation with CpG 1826, anti-Ig, anti CD40, IL-21 and IL-2 (mean ± SD, n = 6).

(B) Extracellular ATP concentrations in cultures of murine B lymphocytes isolated from WT (circle) and *Vamp7* −/− (square) LNs after in vitro stimulation with CpG 1826, anti-ig, anti CD40, IL-21 and IL-2.

(C) Relative decrease in IgG and IgA ISC in *Vamp7* deficient mouse B lymphocytes (open bars) respect to WT B cells (close bars) after in vitro stimulation with CpG 1826 and IL21 or CpG 1826, anti-ig and IL-21. (LNs IgG, n = 2 CpG, IL-21 **p = 0.0085, CpG, anti-ig and IL-21 *p = 0.04; PPs IgG, n = 2-3 CpG, IL-21 *p = 0.03, CpG, anti-ig and IL-21 ****p < 0.0001, PPs IgA, CpG, IL-21 p = 0.053, CpG, anti-ig and IL-21 *p = 0.034).

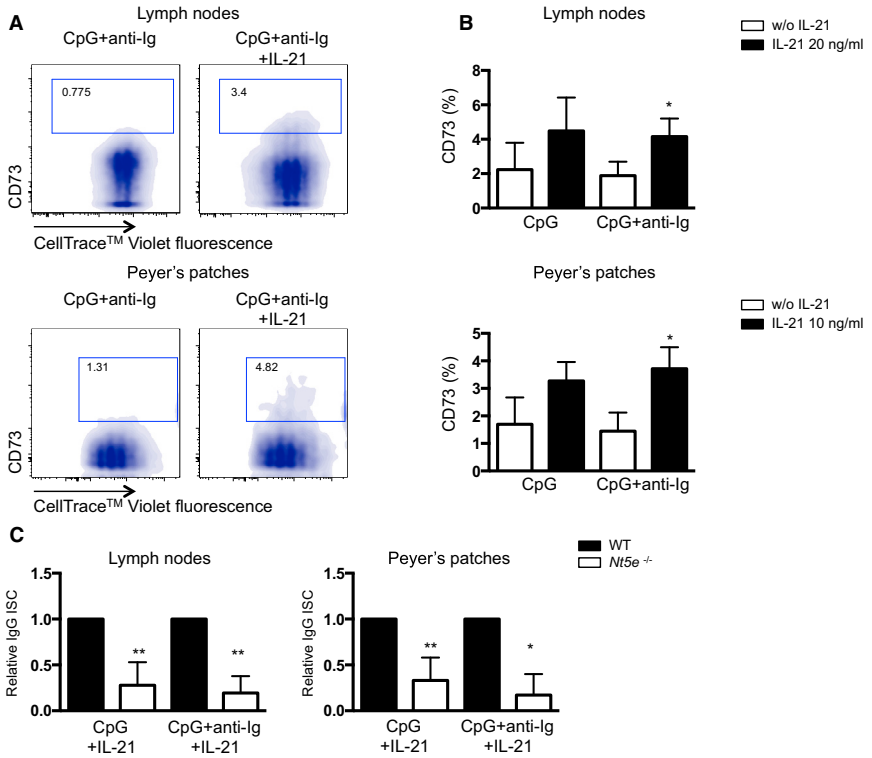

Figure S6. Analysis of Class Switch Recombination in CD73-Deficient Mouse B Lymphocytes, Related to Results and Discussion

(A) Representative dot plots of CD73 expression and cell tracker dilution in naive B cells isolated from LNs and PPs after 5 days of stimulation with CpG and anti-Ig with and without IL-21.

(B) Percentage of CD73 positive cells in LNs and PPs naive B cells after stimulation with CpG alone or in combination with anti-ig with or without IL-21 (n = 5, LNs, CpG, anti-Ig *p = 0.0142, PPs, CpG, anti-ig *p = 0.0193).

(C) Relative decrease of IgG ISC in *Nt5e* deficient naive B cells isolated from LNs and PPs after 5 days of in vitro stimulation with CpG or CpG and anti-ig in the presence of IL-21. (n = 3 LNs IgG, CpG, IL-21 **p = 0.0076, CpG, anti-ig and IL-21 **p = 0.0016, n = 3 PPs IgG CpG, IL-21 **p = 0.0098, CpG, anti-ig and IL-21 *p = 0.036).

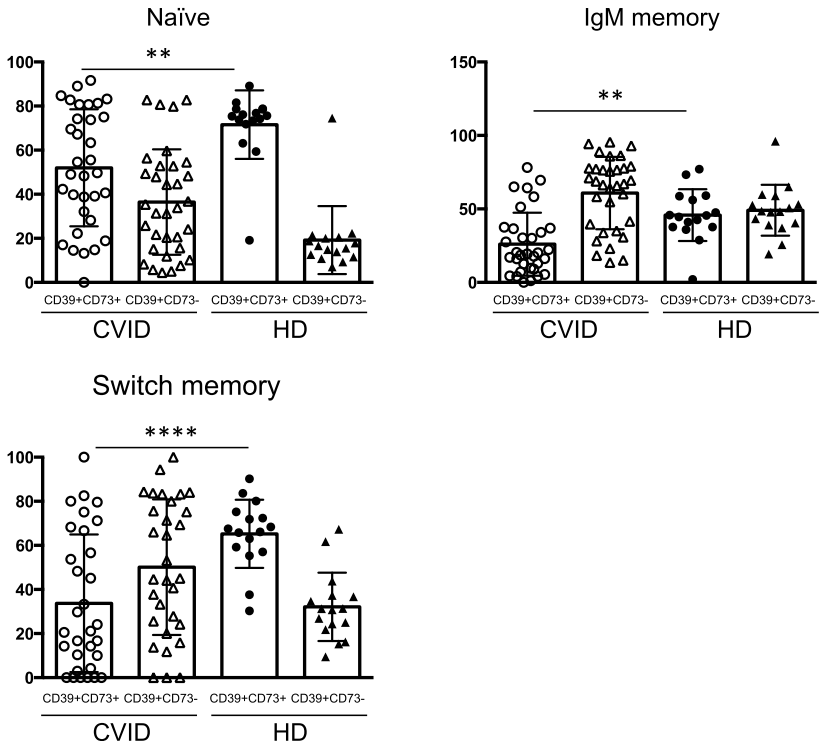

Figure S7. Percentage of CD39$^+$CD73$^+$ in Different Human Peripheral B Cell Subsets in Age-Matched Control and CVID Patients, Related to Results and Discussion

Percentage of CD39$^+$CD73$^+$ and CD39$^+$CD73$^-$ in peripheral B cell subsets, namely naive, IgM memory and switch memory in CVID patients compared with age matched healthy donors (naive CD39$^+$CD73$^+$ CVID versus HD, **$p = 0.022$; IgM memory CD39+CD73+ CVID versus HD, **$p = 0.0015$; switch memory CD39+CD73+ CVID versus HD, ****$p < 0.0001$).

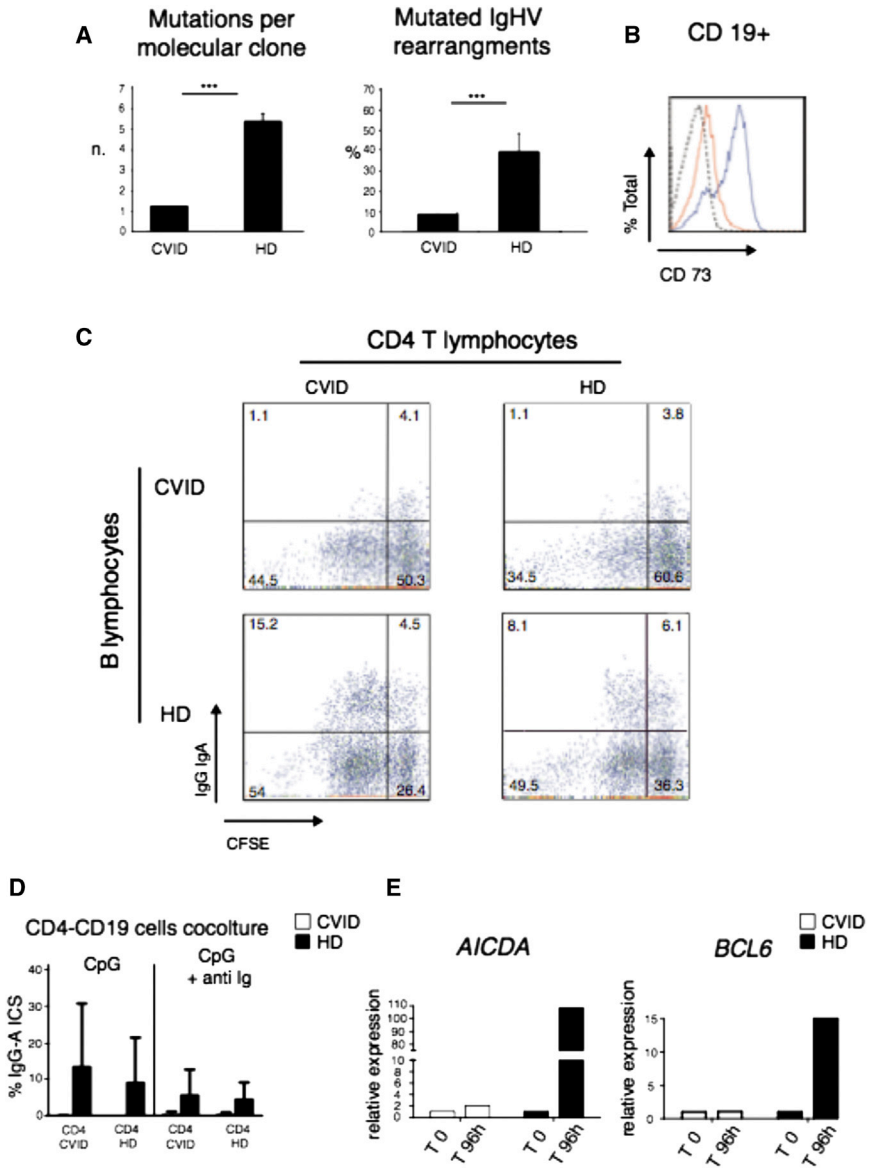

Figure S8. Analysis of Somatic Hypermutation and Class Switch Recombination in B Cells Isolated from CVID Patients, Related to Results and Discussion

(A) Analysis of somatic mutations in a CVID patient and age-matched healthy donor (HD). Left graph shows the number of mutations per clone, right graph displays the percentage of mutated IgHV rearrangments.

(B) Intracellular staining of CD73 in flow cytometry in age-matched HD (blue histogram) and a representative CVID patient (red line). Dotted line depicts staining with isotype-matched antibody in HD.

(C) CFSE dilution and surface IgG/A expression in $CD19^+$ B cells isolated from CVID patient (upper panel) and HD (lower panel) and stimulated with reciprocal irradiated $CD4^+$ T cells in the presence of a combination of bacterial superantigen TSST, CpG 2006 and anti-Ig. Percentages of cells within the quadrants are shown.

(D) Percentage of CVID and HD IgG/A secreting cells in ELISPOT assay relative to total $CD19^+$ cells at 5 days after stimulation as indicated.

(E) mRNA levels for *AICDA* and *BCL6* were determined by quantitative real-time PCR and normalized to the amount of 18S.